Postprint of: Dastjerdi Sh., Malikan M.: Mechanical analysis of eccentric defected bilayer graphene sheets considering the van der Waals force. JOURNAL OF NANOMATERIALS, NANOENGINEERING AND NANOSYSTEMS. (2020).
https://doi.org/10.1177/2397791420926067

Mechanical analysis of eccentric defected bilayer graphene sheets considering the van der Waals force

Shahriar Dastjerdi [a1], Mohammad Malikan[b]

[a]Department of Mechanical Engineering, Shahrood Branch, Islamic Azad University, Shahrood, Iran

[b]Department of Mechanics of Materials and Structures, Faculty of Civil and Environmental Engineering, Gdansk University of Technology, Gdansk, Poland

ABSTRACT

In this paper, it is tried to simulate nonlinear bending analysis of a double-layered graphene sheet (DLGSs) which contains a geometrical imperfection based on an eccentric hole. The first-order shear deformation theory is considered to obtain the governing equations. Also, the nonlinear von Kármán strain field has been assumed in order to obtain large deformations. Whereas the DLGS has been considered, the effect of van der Waals forces has been taken into account in the analysis. In order to implement the nanoscale impact, the nonlocal elasticity theory has been employed. The solution methodology which is here based on the semi-analytical polynomial method (SAPM) solving technique presented previously by the authors, has been applied and again its efficiency has been demonstrated due to its highly accurate results. Due to the fact that this

[1]Corresponding author: Tel: +98-915-5055767

E-mail address: dastjerdi_shahriar@yahoo.com

research has been done for the first time and there is not any validation available, the results of the local single layer sheet are compared with ABAQUS software. The effects of some other parameters on the results have been studied such as the value of eccentricity, van der Waals interaction and nonlocal parameter.

Keywords: Eccentric vacant defect; Nonlocal elasticity theory; First-order shear deformation theory; Bilayer graphene sheet; Van der Waals interaction

Nomenclature

w_1: Defection of upper layer	e: Distance between the center of plate and defect
w_2: Defection of bottom layer	u : In-plane displacement of the plates' nodes along r
r_o: Outer radius of the plate	v : In-plane displacement of the plates' nodes along θ
r_i: Size of defect	w : Transverse displacement of the plates' nodes
ν : Poisson's ratio	ϕ : Rotation of elements around circumferential axis
E : Young's modulus	ψ : Rotation of elements around radial axis
h : Thickness of the each layer	M_r : Moment stress resultant around r axis
k_0 : van der Waals force	M_θ : Circumferential moment stress resultant
q : Static uniform transverse load	$M_{r\theta}$: In-plane moment stress resultant
k_p : Shear layer of elastic matrix	N_θ : Circumferential in-plane stress resultant
k_w : Winkler modulus of elastic matrix	$N_{r\theta}$: Torsional in-plane stress resultant
t: time	N_r : Radial in-plane stress resultant
a: an unknown variable in SAPM	Q_r and Q_θ : Shear stress resultants in two planes
$\mu=(e_0 a)^2$: Nonlocal parameter term	R_v: Ratio of deflection in the presence of defect to the ignoring of defect
R_m: The nonlocal to local analysis	Index i: 1 and 2 for upper and lower layers
ε_r : Radial strain	γ_{rz} : Shear strain in r-z plane
ε_θ : Circumferential strain	$\gamma_{r\theta}$: Shear strain in r- θ plane

z: Thickness coordinate	$\gamma_{\theta z}$: Shear strain in θ-z plan
κ_s : Shear correction factor	∇^2 : Laplace operator

1. Introduction

Double-layered graphene sheets (DLGSs) can be formed from two separated graphene layers which are connected due to the van der Waals interactions between the layers. It is possible to make a bilayer graphene sheet by applying chemical vapor deposition. Many methods have been used to predict the mechanical behavior of nanoscale structures. There are different three methods in this case: atomistic methods, nonlocal continuum methods, and atomistic-continuum methods. If classical mechanics is used, it might lead to considerable errors during the analysis. Between the mentioned theories, nonlocal continuum theory includes several methods as nonlocal elasticity theory [1-3], strain gradient and couple stress theories [4], stress-driven elasticity theory [5, 6], and mixing of the mentioned theories [7, 8], within which the nonlocal elasticity theory is more well-known. Therefore, many researchers have applied this theory to model the mechanical behavior of nanostructures.

In [9, 10] the nonlocal elasticity theory has been presented by Eringen which can be a famous theory in elasticity.

During the last years, many researches have been done to aim to analyze the mechanical behavior of graphene sheets, for example, vibration, buckling and bending analyses. Shen et al. [11] investigated the vibration of single-layered graphene sheet-based nano-mechanical sensor via the nonlocal Kirchhoff plate theory. Zenkour et al. [12] studied thermal analysis of a single-layered graphene sheet (SLGS) embedded in viscoelastic medium. Jiang et al. [13] studied for vibration analysis of single-layered graphene sheet-based mass sensor using Galerkin strip distributed transfer function method.

Dastjerdi et al. [14, 15] investigated the static behavior of monolayer annular/circular and double-layered rectangular nano graphene plate. They received this conclusion that the maximum deflection declines along with the increasing small-scale effects. Dastjerdi and Jabbarzadeh [16] found an approximate single layer equivalent for multi-layer graphene sheets based on nonlocal elasticity theory considering third-order shear deformation theory of the plates (TSDT). Liu et al. [17] discussed the effects of defects on the chemical, electronic, magnetic, and mechanical properties of graphene and addressed the associated challenges and prospects on the future study of defects in graphene and other nanocarbon materials. Dastjerdi et al. [18] derived the constitutive equations of nanoplates embedded in elastic matrix based on Eringen nonlocal elasticity theory and applied both first-order shear deformation theory (FSDT) and higher-order shear deformation theory (HSDT) theory. Moreover, Dastjerdi et al. [19] investigated the eccentric defected mono-layer graphene sheets embedded in an elastic matrix. They found that the types of boundary conditions and small-scale effects can affect the results. And also, the value of eccentricity can be added too. Malikan et al. [20] considered bilayer graphene sheets bridged on the elastic medium of Pasternak and analyzed the shear and thermal stability resistance of the FSDT modeled system. Ma et al. [21] studied the effects of magnetic field on thin composite films. They considered bilayer thin films in their analysis and used the Heisenberg model to describe the bilayer film structure. Naderi and Saidi [22] developed the nonlocal constitutive equations of nanostructures. They showed that nonlocal theories could not be used in the presence of surface effects. Mohammadimehr et al. [23] investigated the effects of surface stress on the bending and vibration analyses of SLGSs sheets embedded on an elastic foundation using the energy method. Karimi and Shahidi [24] studied thermo-mechanical bending, vibration and buckling analysis of orthotropic graphene sheets using refined nonlocal elasticity theory. They also considered the effects of

surface energy in their analysis. Ansari et al. [25] examined the stability of SLGSs with different boundary conditions using nonlocal elasticity theory. They evaluated the axial buckling analysis in their study. Lu et al. [26] analyzed the vibration and natural frequencies of a multi-layered graphene sheet based on the classical plate theory and analytical solutions. They investigated the influences of various layerwise tension forces. In a special research, Nazemnezhad et al. [27] modeled the multi-layered graphene sheets (MLGSs)) as a sandwich plate via molecular dynamic simulation (MD) and estimated the interlayer shear effects. They confirmed that modelling a MLGS with sandwich plate can result in a highly accurate prediction. Wu and Li [28] formulated a multiple time scale method to analyze the SLGSs embedded in the Pasternak foundation on the basis of Eringen nonlocal elasticity model. In a crucial study, Allahyari and Asgari [29] developed a nonlocal higher-order shear deformation theory to consider vibrations of a DLGS placed in an elastic matrix and thermal environment and also studied the surface effects. Hashemi et al. [30] combined the internal viscosity to the elastic model of DLGSs and evaluated the natural frequencies while the DLGS was rested in a Pasternak medium. The classical plate hypothesis was in conjunction with linear Lagrangian strains as well as nonlocal elasticity theory of Eringen to present the desired mathematical relations. In an applicable research, Ansari et al. [31] conducted use of MD to study some vacancy defects in a rectangular SLGS. More importantly, they investigated fracture in the model. Wang et al. [32] based on the analytical results, discussed the effects of thermal on natural frequencies of a DLGS on the basis of nonlocal elasticity model. In a particular work, Allahyari and Asgari [33] presented a nonlinear wave propagation analysis on the SLGS with assuming circular geometry. Moreover, the effects of environments such as magnetic and temperature were also taken into consideration. They utilized the nonlocal elasticity as well as the modified couple stress theory to justify the small scale influences. Giannopoulos and Avntoulla

[34] analyzed crack and crack features on the tensile strength of graphene in thermal environment by means of MD. In another valuable research, Giannopoulos [35] estimated a circular graphene sheet involving a crack under a vibrational situation using a structural mechanics method in a three-dimensional spring-based domain on the basis of the atomistic models.

The irregularity in the atomic scale structure can occur in the two-dimensional (2D) plane graphene sheet during the manufacturing and production process. We can assume that the graphene sheet is also defective in its atomic scale. Such the irregularity in graphene sheets can be classified in some cases as a heterogeneous defect, topological defects (non-hexagonal shape of arranging atoms) and bonding defects (atoms dislocations, and vacancies) [36-38]. In this paper, the term defect is referred to as the vacancy and missing carbon atoms as a material deviation. In graphene, when one or more carbon atoms are missed, there cannot be a bond between surrounding atoms and some bonds remain in a dangling manner [39] (Fig. 1b).

Studying of defected monolayer circular graphene sheet has been done before by the authors. However, it is too hard to find monolayers in reality. So, in this paper, the bilayer sheet is considered and nonlocal elasticity theory has been applied to obtain the governing equations including the van der Waals interaction between the layers. The position of defect is moving and it is not placed at the center so the axisymmetric problem has been obtained. The obtained equations are solved by applying SAPM for which the efficiency is proved again. Whereas there are not any works available in this case, the results are obtained for different locations of defect, and van der Waals interaction. The results are compared with ABAQUS software as well and good agreements have been achieved after this calculation. Finally, the effects of eccentricity, van der Waals interaction and small-scale influences on the results have been studied.

2. Constitutive Equations and solution

Analysis of single layer defected graphene sheet was studied earlier [19]. In Fig. 1. a double-layered graphene plate is considered which contains an internal eccentric hole. The bilayer sheet is embedded in Winkler-Pasternak elastic medium. The values of Winkler and Pasternak stiffness are k_w and k_p respectively. In addition, k_o refers to the amount of van der Waals interaction between the layers.

Stacking and layering the graphene as 2D sheets of graphite with chemical functionalization make bilayer and multilayer graphene sheets. There is a weak connection between layers when we compared the bonding with the connections of atoms in the plane. One can distinguish this weak bonding can be the van der Waals forces. As a rule, the induced electric polarity makes such bonding. There is no thermal or electrical conductivity along the bonding [40]. In an atomic analysis, the van der Waals forces are attained with respect to a derivative of Lennard-Jones pair potential [41]. One can find that this force is a nonlinear function of interatomic distance. However, the nonlinearity in the behavior of van der Waals forces can be important while we analyze in-phase or out-phase for bilayer graphene sheet and as far as we assumed both layers are rigid together, it seems not important to consider nonlinearly the van der Waals forces. As the van der Waals force is based on the Taylor expansion, we only used the first term of this expansion leads to a linear expression. When using Taylor expansion for the van der Waals force and integrating it over the 2D sheet of graphene, the van der Waals bonding force between upper and lower sheets could be achieved [41, 42]. The distance between two layers is 0.331 nm ≤ distance ≤ 0.35 nm depending on how the layers are stacking on each other while both the layers are normally in an equilibrium condition [41-43].

To access the value of the van der Waals coefficient, the distance between layers plays a major role and the amount of this force directly related to the distance [44]. As mentioned by [43,

44], the value of van der Waals force can be varied numerically in unit GPa/nm for linear expressions and GPa/nm^3 for nonlinear ones. Note that the positive sign for van der Waals force represents the attraction of atoms and the negative sign depicts repulsion. As the scope of this paper is only considering the vacancy imperfection into the DLGSs, hence, we ignore the exact values of the van der Waals coefficient and an arbitrary value is in use whilst it results in rigidity behavior of both layers.

In this study, the van der Waals interaction is simulated by linear spring as $k_o\left(w_2-w_1\right)$. With regard to the Fig. 1a and b, geometric parameters of the defect are *S*, and *e*, and the relation between the distance of the center of eccentric defect from outer boundary is $S=e\left(\sqrt{\left(\frac{r_o}{e}\right)^2-\sin^2(\theta)}+\cos(\theta)\right)$.

The mathematical expressions of strain-displacement by means of FSDT can be appeared in the nonlinear view as

$$\varepsilon_r=\frac{\partial u}{\partial r}+z\frac{\partial \phi}{\partial r}+\frac{1}{2}\left(\frac{\partial w}{\partial r}\right)^2 \tag{1}$$

$$\varepsilon_\theta=\frac{1}{r}\left(\frac{\partial v}{\partial \theta}+u\right)+\frac{z}{r}\left(\frac{\partial \psi}{\partial \theta}+\phi\right)+\frac{1}{2}\left(\frac{1}{r}\frac{\partial w}{\partial \theta}\right)^2 \tag{2}$$

$$\gamma_{rz}=\frac{\partial w}{\partial r}+\phi \tag{3}$$

$$\gamma_{\theta z}=\frac{1}{r}\frac{\partial w}{\partial \theta}+\psi \tag{4}$$

$$\gamma_{r\theta}=\frac{1}{r}\left(\frac{\partial u}{\partial \theta}+z\frac{\partial \phi}{\partial \theta}-v-z\psi\right)+\frac{\partial v}{\partial r}+z\frac{\partial \psi}{\partial r}+\frac{1}{r}\frac{\partial w}{\partial r}\frac{\partial w}{\partial \theta} \tag{5}$$

The governing equations for the bilayer graphene sheet on the basis of Eqs. (1)-(5), and Hamiltonian, can be presented by neglecting some inconsiderable terms as follows [18] (*i*=1, 2):

$$\delta ui : Ni_{r,r} + \frac{1}{r}\left(Ni_{r\theta,\theta} + Ni_r - Ni_\theta\right) = 0 \tag{6}$$

$$\delta vi : Ni_{r\theta,r} + \frac{1}{r}\left(Ni_{\theta,\theta} + 2Ni_{r\theta}\right) = 0 \tag{7}$$

$$\begin{aligned}&\delta w1 : Q1_{r,r} + \frac{1}{r}\left(Q1_{\theta,\theta} + Q1_r\right) + q + k_o(w2 - w1) + N1_r \frac{\partial^2 w1}{\partial r^2} \\ &+ N1_\theta\left(\frac{1}{r}\frac{\partial w1}{\partial r} + \frac{1}{r^2}\frac{\partial^2 w1}{\partial \theta^2}\right) + 2N1_{r\theta}\left(\frac{1}{r}\frac{\partial^2 w1}{\partial r \partial \theta} - \frac{1}{r^2}\frac{\partial w1}{\partial \theta}\right) = 0\end{aligned} \tag{8}$$

$$\begin{aligned}&\delta w2 : Q2_{r,r} + \frac{1}{r}\left(Q2_{\theta,\theta} + Q2_r\right) - k_o(w2 - w1) - k_w w2 + k_p \nabla^2 w2 + \\ &N2_r \frac{\partial^2 w2}{\partial r^2} + N2_\theta\left(\frac{1}{r}\frac{\partial w2}{\partial r} + \frac{1}{r^2}\frac{\partial^2 w2}{\partial \theta^2}\right) + 2N2_{r\theta}\left(\frac{1}{r}\frac{\partial^2 w2}{\partial r \partial \theta} - \frac{1}{r^2}\frac{\partial w2}{\partial \theta}\right) = 0\end{aligned} \tag{9}$$

$$\delta \phi i : Mi_{r,r} + \frac{1}{r}\left(Mi_{r\theta,\theta} + Mi_r - Mi_\theta\right) - Qi_r = 0 \tag{10}$$

$$\delta \psi i : Mi_{r\theta,r} + \frac{1}{r}\left(Mi_{\theta,\theta} + 2Mi_{r\theta}\right) - Qi_\theta = 0 \tag{11}$$

in which

$$Ni_r = \frac{Eh}{1-\nu^2}\left(\frac{\partial ui}{\partial r} + \frac{1}{2}\left(\frac{\partial wi}{\partial r}\right)^2 + \nu\left(\frac{ui}{r} + \frac{1}{r}\frac{\partial vi}{\partial \theta} + \frac{1}{2}\left(\frac{1}{r}\frac{\partial wi}{\partial \theta}\right)^2\right)\right) \tag{12}$$

$$Ni_\theta = \frac{Eh}{1-\nu^2}\left(\nu\left(\frac{\partial ui}{\partial r} + \frac{1}{2}\left(\frac{\partial wi}{\partial r}\right)^2\right) + \frac{ui}{r} + \frac{1}{r}\frac{\partial vi}{\partial \theta} + \frac{1}{2}\left(\frac{1}{r}\frac{\partial wi}{\partial \theta}\right)^2\right) \tag{13}$$

$$Ni_{r\theta} = \frac{Eh}{2(1+\nu)}\left(\frac{\partial vi}{\partial r} - \frac{vi}{r} + \frac{1}{r}\frac{\partial ui}{\partial \theta} + \frac{1}{r}\frac{\partial wi}{\partial r}\frac{\partial wi}{\partial \theta}\right) \tag{14}$$

$$Qi_r = \frac{\kappa_s Eh}{2(1+\nu)}\left(\frac{\partial wi}{\partial r} + \phi i\right) \tag{15}$$

$$Qi_\theta = \frac{\kappa_s Eh}{2(1+\nu)}\left(\frac{1}{r}\frac{\partial wi}{\partial \theta} + \psi i\right) \tag{16}$$

$$Mi_r = \frac{Eh^3}{12(1-\nu^2)}\left(\frac{\partial \phi i}{\partial r} + \frac{\nu}{r}\left(\frac{\partial \psi i}{\partial \theta} + \phi i\right)\right) \tag{17}$$

$$Mi_\theta = \frac{Eh^3}{12(1-\nu^2)}\left(\nu\frac{\partial \phi i}{\partial r} + \frac{1}{r}\left(\frac{\partial \psi i}{\partial \theta} + \phi i\right)\right) \tag{18}$$

$$M_{r\theta} = \frac{Eh^3}{24(1+\nu)}\left(\frac{\partial \psi i}{\partial r} + \frac{1}{r}\frac{\partial \phi i}{\partial \theta} - \frac{\psi i}{r}\right) \tag{19}$$

As this paper is concerned with Eringen's nonlocal elasticity theory to implement the small scale effects, the nonlocal stress can be appeared as [14, 45-48]

$$\left(1-\mu\nabla^2\right)\sigma_{ij} = C_{ijkl}\varepsilon_{kl} \tag{20}$$

Therefore, applying Eq. (20) on Eqs. (12)-(19) and re-writing Eqs. (6)-(11), one can get

$$Ni_{r,r} + \frac{1}{r}\left(Ni_{r\theta,\theta} + Ni_r - Ni_\theta\right) = 0 \tag{21}$$

$$Ni_{r\theta,r} + \frac{1}{r}\left(Ni_{\theta,\theta} + 2Ni_{r\theta}\right) = 0 \tag{22}$$

$$\begin{aligned} &Q1_{r,r} + \frac{1}{r}\left(Q1_{\theta,\theta} + Q1_r\right) + \left(1-\mu\nabla^2\right)\left(q + k_o(w2-w1) + N1_r\frac{\partial^2 w1}{\partial r^2}\right. \\ &\left. + N1_\theta\left(\frac{1}{r}\frac{\partial w1}{\partial r} + \frac{1}{r^2}\frac{\partial^2 w1}{\partial \theta^2}\right) + 2N1_{r\theta}\left(\frac{1}{r}\frac{\partial^2 w1}{\partial r\partial\theta} - \frac{1}{r^2}\frac{\partial w1}{\partial \theta}\right)\right) = 0 \end{aligned} \tag{23}$$

$$\begin{aligned} &Q2_{r,r} + \frac{1}{r}\left(Q2_{\theta,\theta} + Q2_r\right) + \left(1-\mu\nabla^2\right)\left(-k_o(w2-w1) - k_w w2 + k_p\nabla^2 w2 + \right. \\ &\left. N2_r\frac{\partial^2 w2}{\partial r^2} + N2_\theta\left(\frac{1}{r}\frac{\partial w2}{\partial r} + \frac{1}{r^2}\frac{\partial^2 w2}{\partial \theta^2}\right) + 2N2_{r\theta}\left(\frac{1}{r}\frac{\partial^2 w2}{\partial r\partial\theta} - \frac{1}{r^2}\frac{\partial w2}{\partial \theta}\right)\right) = 0 \end{aligned} \tag{24}$$

$$Mi_{r,r} + \frac{1}{r}\left(Mi_{r\theta,\theta} + Mi_r - Mi_\theta\right) - Qi_r = 0 \tag{25}$$

$$Mi_{r\theta,r} + \frac{1}{r}\left(Mi_{\theta,\theta} + 2Mi_{r\theta}\right) - Qi_\theta = 0 \tag{26}$$

Based on the Eqs. (12)-(19), Eqs. (21)-(26) would be attained into displacements as below (Note

that in order to shorten and summarize, as Eqs. (23) and (24) are too long, they are not transferred into the displacement mode)

$$\begin{aligned}
&\frac{Eh}{1-\nu^2}\left(\frac{\partial^2 ui}{\partial r^2}+\frac{\partial^2 wi}{\partial r^2}\frac{\partial wi}{\partial r}+\nu\left(\frac{1}{r}\frac{\partial ui}{\partial r}-ui\frac{1}{r^2}+\frac{1}{r}\frac{\partial^2 vi}{\partial r\partial\theta}-\frac{1}{r^2}\frac{\partial vi}{\partial\theta}+-\frac{1}{r^2}\frac{\partial wi}{\partial\theta}+\frac{1}{r}\frac{\partial^2 wi}{\partial r\partial\theta}\right)\right)\\
&+\frac{Eh}{2r(1+\nu)}\left(\frac{\partial^2 vi}{\partial r\partial\theta}-\frac{1}{r}\frac{\partial vi}{\partial\theta}+\frac{1}{r}\frac{\partial^2 ui}{\partial\theta^2}+\frac{1}{r}\frac{\partial wi}{\partial r}\frac{\partial^2 wi}{\partial\theta^2}++\frac{1}{r}\frac{\partial^2 wi}{\partial r\partial\theta}\frac{\partial wi}{\partial\theta}\right)\\
&+\frac{Eh}{r\left(1-\nu^2\right)}\left(\frac{\partial ui}{\partial r}+\frac{1}{2}\left(\frac{\partial wi}{\partial r}\right)^2+\nu\left(\frac{ui}{r}+\frac{1}{r}\frac{\partial vi}{\partial\theta}+\frac{1}{2}\left(\frac{1}{r}\frac{\partial wi}{\partial\theta}\right)^2\right)\right)\\
&-\frac{Eh}{r\left(1-\nu^2\right)}\left(\nu\left(\frac{\partial ui}{\partial r}+\frac{1}{2}\left(\frac{\partial wi}{\partial r}\right)^2\right)+\frac{ui}{r}+\frac{1}{r}\frac{\partial vi}{\partial\theta}+\frac{1}{2}\left(\frac{1}{r}\frac{\partial wi}{\partial\theta}\right)^2\right)=0
\end{aligned} \tag{27}$$

$$\begin{aligned}
&\frac{Eh}{2(1+\nu)}\left(\frac{\partial^2 vi}{\partial r^2}-\frac{1}{r}\frac{\partial vi}{\partial r}+\frac{vi}{r^2}-\frac{1}{r^2}\frac{\partial ui}{\partial\theta}+\frac{1}{r}\frac{\partial^2 ui}{\partial r\partial\theta}-\frac{1}{r^2}\frac{\partial wi}{\partial r}\frac{\partial wi}{\partial\theta}+\frac{1}{r}\frac{\partial^2 wi}{\partial r\partial\theta}\frac{\partial wi}{\partial\theta}+\frac{1}{r}\frac{\partial^2 wi}{\partial r^2}\frac{\partial wi}{\partial\theta}\right)\\
&+\frac{Eh}{r\left(1-\nu^2\right)}\left(\nu\left(\frac{\partial^2 ui}{\partial r\partial\theta}+\frac{\partial wi}{\partial r}\frac{\partial^2 wi}{\partial r\partial\theta}\right)+\frac{1}{r}\frac{\partial ui}{\partial\theta}+\frac{1}{r}\frac{\partial^2 vi}{\partial\theta^2}+\frac{1}{r}\frac{\partial wi}{\partial\theta}\frac{\partial^2 wi}{\partial\theta^2}\right)\\
&+\frac{Eh}{r(1+\nu)}\left(\frac{\partial vi}{\partial r}-\frac{vi}{r}+\frac{1}{r}\frac{\partial ui}{\partial\theta}+\frac{1}{r}\frac{\partial wi}{\partial r}\frac{\partial wi}{\partial\theta}\right)=0
\end{aligned} \tag{28}$$

$$\begin{aligned}
&\frac{Eh^3}{12(1-\nu^2)}\left(\frac{\partial^2\phi i}{\partial r^2}-\frac{\nu}{r^2}\left(\frac{\partial\psi i}{\partial\theta}+\phi i\right)+\frac{\nu}{r}\left(\frac{\partial^2\psi i}{\partial r\partial\theta}+\frac{\partial\phi i}{\partial r}\right)\right)\\
&+\frac{Eh^3}{24r\left(1+\nu\right)}\left(\frac{\partial^2\psi i}{\partial r\partial\theta}+\frac{1}{r}\frac{\partial^2\phi i}{\partial\theta^2}-\frac{1}{r}\frac{\partial\psi i}{\partial\theta}\right)+\frac{Eh^3}{12r(1-\nu^2)}\left(\frac{\partial\phi i}{\partial r}+\frac{\nu}{r}\left(\frac{\partial\psi i}{\partial\theta}+\phi i\right)\right)\\
&-\frac{Eh^3}{12r(1-\nu^2)}\left(\nu\frac{\partial\phi i}{\partial r}+\frac{1}{r}\left(\frac{\partial\psi i}{\partial\theta}+\phi i\right)\right)-\frac{\kappa_s Eh}{2(1+\nu)}\left(\frac{\partial wi}{\partial r}+\phi i\right)=0
\end{aligned} \tag{29}$$

$$\begin{aligned}
&\frac{Eh^3}{24\left(1+\nu\right)}\left(\frac{\partial^2\psi i}{\partial r^2}-\frac{1}{r^2}\frac{\partial\phi i}{\partial\theta}+\frac{1}{r}\frac{\partial^2\phi i}{\partial r\partial\theta}+\frac{\psi i}{r^2}-\frac{1}{r}\frac{\partial\psi i}{\partial r}\right)-\frac{\kappa_s Eh}{2(1+\nu)}\left(\frac{1}{r}\frac{\partial wi}{\partial\theta}+\psi i\right)\\
&+\frac{Eh^3}{12r(1-\nu^2)}\left(\nu\frac{\partial^2\phi i}{\partial r\partial\theta}+\frac{1}{r}\left(\frac{\partial^2\psi i}{\partial\theta^2}+\frac{\partial\phi i}{\partial\theta}\right)\right)+\frac{Eh^3}{12r\left(1+\nu\right)}\left(\frac{\partial\psi i}{\partial r}+\frac{1}{r}\frac{\partial\phi i}{\partial\theta}-\frac{\psi i}{r}\right)=0
\end{aligned} \tag{30}$$

Taking a look at the governing equations, it is clear that a two-dimensional solving process must be considered in which its solution is not possible by common analytical methods. In the paper, due to eccentricity and axisymmetric nonlinear problems, applying common analytical and

numerical methods are not possible, hence SAPM method which is presented by the authors [14, 49] before is applied again. According to the previous work, the polynomial functions can be presented below: (i=1, 2)

$$ui = \sum_{k=1}^{N}\sum_{t=1}^{M} ai_{\left(k+t-\left(1-(k-1)(M-1)\right)\right)} r^{(k-1)}\theta^{(t-1)} \tag{31}$$

$$vi = \sum_{k=1}^{N}\sum_{t=1}^{M} ai_{\left(k+t-\left(1-(k-1)(M-1)\right)+M\cdot N\right)} r^{(k-1)}\theta^{(t-1)} \tag{32}$$

$$wi = \sum_{k=1}^{N}\sum_{t=1}^{M} ai_{\left(k+t-\left(1-(k-1)(M-1)\right)+2M\cdot N\right)} r^{(k-1)}\theta^{(t-1)} \tag{33}$$

$$\phi i = \sum_{k=1}^{N}\sum_{t=1}^{M} ai_{\left(k+t-\left(1-(k-1)(M-1)\right)+3M\cdot N\right)} r^{(k-1)}\theta^{(t-1)} \tag{34}$$

$$\psi i = \sum_{k=1}^{N}\sum_{t=1}^{M} ai_{\left(k+t-\left(1-(k-1)(M-1)\right)+4M\cdot N\right)} r^{(k-1)}\theta^{(t-1)} \tag{35}$$

By considering the above polynomial equations, the constitutive equations are transformed into algebraic equations system and might be solved conveniently. The obtained equations can be solved by the definition of boundary conditions.

3. Numerical results

Owing to this problem that there is no available study on the effect of eccentric defects, the obtained results of the monolayer macro sheet based on local theory considering different eccentricity values are validated with ABAQUS in Table 1. To assess the problem in FEM, we use a nonlinear triangular element. Moreover, the boundary conditions in the software were taken as CC and CF, which the first character relates to the outer diameter and the second one dedicates to the inner diameter. Generally, in this paper the C boundary condition means clamped and the F means free edges. The SAPM method is approximately 40 percent faster than ABAQUS by

considering high number of elements. Also, the nonlocal results of this paper for an annular/circular graphene sheet is compared with Ref [14] in Table 2. The insignificant differences between the results of this paper and Ref [14] are observed because this paper is two-dimensional analysis and Ref [14] is one dimensional. It is observed that the achieved results are similar to the results of ABAQUS and Ref [14]. Consequently, the SAPM gives acceptable results in this case and it could be possible to validate the obtained results of the mentioned method with the other references. The geometry and material properties of the sheet could be seen below (Table 1):

$$r_i = 0.1\text{m}; r_o = 0.5\text{m}; h = 0.01\text{m}; E = 1.9\times10^{11}\,\text{N/m}^2; \nu = 0.29; q = 10^4\,\text{Pa}$$

In Fig. 2, deflection of two layers versus the van der Waals interaction between two layers are compared. The plate specifications are as follows [19]:

$$r_i = 1\text{nm}; r_o = 5\text{nm}; h = 0.34\text{nm}; e = 1\text{nm}; E = 1.06\text{TPa}; \nu = 0.3; q = 0.1\text{GPa}$$
$$k_w = 1.13\text{GPa/nm}; k_p = 1.13\text{Pa.m}$$

According to Fig. 2, it is observed that by raising the van der Waals interaction between two layers, the deflection of the upper layer decreases and for the bottom layer increases. In the following, by raising van der Waals force, deflections of both layers reach to each other, in continue, no significant differences can be seen. It can be noted that the van der Waals force between layers is dependent on the distance between layers and usually is taken k_o = 40 GPa/nm. As Fig. 2 is shown, by raising the nonlocal parameter the deflections of both upper and bottom layers reach each other by small values of k_o coefficient, and it has resulted that by raising nonlocal coefficient, the effect of van der Waals interaction between layers will be increased.

Fig. 3 is plotted to show the effect of R_m. As it is observed, for the upper layer, deflection in the nonlocal case is always less than the local one. On the other hand, for the upper layer which $R_m < 1$, by raising k_o or raising van der Walls force up to a specified value of k_o, two nonlocal and

local analyses are far from each other and slope of the curve is steep. However, hereinafter by raising k_o, R_m is constant without any effect, and the slope of the curve is approximately zero. Then, it is observed that by raising nonlocal coefficient, differences of nonlocal and local theories become more than before; however, without any effect on the mentioned k_o which hereinafter variation of R_m becomes approximately zero. Also, the results of e_0a =1 nm and e_0a = 2 nm are similar as well. As it is shown in Fig. 3, for the bottom layer up to a specified k_o on the contrary of the upper layer which deflection of nonlocal is less than local case, deflection of nonlocal is more than local. The rate of falling R_m for the bottom layer is similar to the upper layer, but the slope of variations is less than the upper layer. Finally, it is observed that by raising k_o, R_m for both upper and bottom layers is identical, and after a specified k_o, no change in R_m occurs, and the specified k_o for two nonlocal cases of e_0a =1 nm and e_0a = 2 nm is approximately similar.

Fig. 4 (a) and (b) show the diagram of deflection variations of the plate with CC boundary conditions versus raising eccentricity for different values of elastic medium Winkler-Pasternak. Taking a look at diagrams, it is concluded that the deflection of both upper and bottom layers will be increased by raising eccentricity e. Also, by raising k_w and k_p as it is expected, the deflection will be decreased, but it is considered that by raising k_p the deflection of the plate is reduced a little more than the case with just Winkler medium. Therefore, in this example, the Pasternak medium has more effect on the decrease of deflection. Slopes of both diagrams of Fig. 4 are approximately similar and it has resulted that the effects of raising eccentricity e for both Winkler and Pasternak are the same with a slight deviation. According to the diagrams, it is observed that by raising k_w and k_p, the rate of variation is decreased. On the other hand, the effect of eccentricity e is decreased and it is concluded that in high values of k_w and k_p, the effect of raising of eccentricity e on results becomes very smaller than before. Also, by raising k_w and k_p, deviation of two upper

and bottom layers is increased, due to the bottom layer embedded on elastic medium and the upper layer is under transverse loading. As well as raising k_w and k_p, deflection of the bottom layer rather than the upper layer is reduced more, therefore deviation of deflection for both layers is heightened.

In Fig. 5, the diagram shows variation of deflection versus raising eccentricity *e*, considering different nonlocal coefficients (CC boundary conditions). According to Fig. 5, as the same as Fig. 4 (a) and (b), it is observed that by raising eccentricity *e*, deflections of both layers are raised. Again, by raising nonlocal coefficient, deflections of both layers get similar to each other, but no considerable changes in the slope of diagrams are observed. Further to the mentioned paragraphs, by raising nonlocal coefficient, deflections of both layers get closer and it has resulted that the nonlocal coefficient effects on van der Waals interaction between layers is increased which leads to strengthening the force between the layers.

Fig. 6 shows the effect of nonlocal analysis versus moving defect. It is observed that by raising eccentricity *e*, variations of R_m are very small. Distinctly, for the upper layer, the changes are very small and ignorable, but for bottom layer the variations are considerable and it is observed that by raising eccentricity *e*, R_m is decreased and approaches to the value for the upper layer. Therefore, in graphene sheets with two layers, it can be seen that by raising or decreasing the position of defect, no considerable change in the nonlocal analysis is attained. For example, if nonlocal deflection in small values of eccentricity *e* is available, the deflection of the plate for higher values of eccentricity (*e*) could be predicted as well. In particular, with increasing the eccentricity of defect, by increasing anti-symmetric specification, the numerical analysis will be more complicated, and according to Fig. 6, the resulted values of small *e* could be utilized for obtaining results of the cases with larger *e*.

To study the effect of the existence of the defect, Fig. 7 is presented. As it is observed, by

raising the nonlocal coefficient, the value of R_v is decreased, so increasing the small-scale effects leads to reducing the effect of availability of defect. Another result according to Fig. 7 can be mentioned that the variation of R_v for the bottom layer is severely more than the upper layer. For the bottom layer, at the start of growing the nonlocal coefficient, the variations are severe, but for the upper layer is vice versa and the variations are small. Also, for the bottom layer, the slope of variations is decreased and by the manner, along the raise of nonlocal coefficient, R_v is increased approximately similar for both upper and bottom layers.

The effect of defect size in a bilayer defected circular graphene sheet is studied. Fig. 8 is presented in this regard. As it is demonstrated, by increasing defect size, the deflection of the plate is decreased. At first, the variations are severe, but in continue, the variations are decreased. Also, by raising the nonlocal coefficient, as it has resulted before, it is observed that deflection of both upper and bottom layers tends to each other but the slope of variations of two layers are similar and increase of defect size has the same effect on the results of upper and bottom layers.

Finally, the nonlinear analysis has been conducted on the research. The nonlinear terms in the strain field lead to more accurate results for large deflections. Whatever the amount of loading imposed on the sheet surface intensifies, the large deflection will be produced. Consequently, the deflection variation of upper and bottom layers versus loading is attended. Fig. 9 shows the comparison between the linear and nonlinear analyses for a defected bilayer graphene sheet. It is observed that for lower amounts of loadings both linear and nonlinear analyses are identical. However, as the loading increases, the differences between linear and nonlinear studies will be more significant. The linear analysis gives the same increment of the results for the same variation of loading, absolutely on the contrary in nonlinear analysis. The differences between linear and nonlinear analyses are more considerable for the upper layer deflection rather than the bottom

layer. According to Fig. 9, it is concluded that if the sheet is under high loading, the linear analysis causes serious errors and the obtained results are not acceptable and the nonlinear analysis must be applied instead. The nonlinear analysis will be more complicated and increases the number of calculations dramatically; however, as stated before it gives more accurate results. Consequently, in this paper, the nonlinear analysis has been attended.

4. Conclusions

In the present study, the nonlinear bending behavior of double-layered defected graphene sheets is studied based on nonlocal elasticity theory while the plate is rested in an elastic matrix. The governing equations are derived by considering the van der Waals interaction between the layers. The constitutive equations are solved using SAPM which was presented by authors before. The main out-comings of the article can be summarized as follows:

- SAPM which is a semi-analytical method gives appropriate results in comparison with the other numerical methods.
- By raising the nonlocal coefficient, the effect of van der Waals interaction between the layers will be increased.
- The results are dependent on the value of Winkler and Pasternak elastic foundations. Whatever the defect reaches to the edges, the effect of Winkler and Pasternak elastic mediums are approximately the same, however, the Winkler foundation's effect is inconsiderably more than Pasternak.
- The value of eccentricity has the same effects on the results for different values of the nonlocal parameter.
- The increase of defect size has the same effects on the results of the upper and bottom layers.

- The presence of the defect affects the upper layer's deflection significantly more than the bottom layer.
- The small-scale effect decreases with the growth of the defect.
- Nonlinear analysis gives more accurate results especially for large deflections in which the linear results are not acceptable.

References

[1] Pradhan, SC, Phadikar, JK. Small scale effect on vibration of embedded multilayered graphene sheets based on nonlocal continuum models. Phys Lett A 2009; 373: 1062-1069.

[2] Dastjerdi, Sh, Akgöz, A. New static and dynamic analyses of macro and nano FGM plates using exact three-dimensional elasticity in thermal environment. Compos Struct 2018; 192: 626-641.

[3] Dastjerdi, Sh, Akgöz, A. On the statics of fullerene structures. Int J Eng Sci 2019; 142: 125-144.

[4] Malikan, M. Electro-mechanical shear buckling of piezoelectric nanoplate using modified couple stress theory based on simplified first order shear deformation theory. Appl Math Model 2017; 48: 196-207.

[5] Barretta, R, Caporale, A, Faghidian, SA, Luciano, R, Marotti de Sciarra, F, Medaglia, CM. A stress-driven local-nonlocal mixture model for Timoshenko nano-beams. Compos Part B-Eng 2019; 164: 590-598.

[6] Sedighi, HM, Malikan, M. Stress-driven nonlocal elasticity for nonlinear vibration characteristics of carbon/boron-nitride hetero-nanotube subject to magneto-thermal environment. Phys Scripta 2020, https://doi.org/10.1088/1402-4896/ab7a38

[7] Malikan, M, Krasheninnikov, M, Eremeyev, VA. Torsional stability capacity of a nano-composite shell based on a nonlocal strain gradient shell model under a three-dimensional magnetic field. Int J Eng Sci 2020; 148: 103210.

[8] Malikan, M, Nguyen, VB. Buckling analysis of piezo-magnetoelectric nanoplates in hygrothermal environment based on a novel one variable plate theory combining with higher-order nonlocal strain gradient theory. Physica E 2018; 102: 8-28.

[9] Eringen, AC. Nonlocal continuum mechanics based on distributions", Int J Eng Sci 2006; 44: 141–147.

[10] Eringen, A.C. Nonlocal continuum field theories, New York: Springer-Verlag 2002.

[11] Shen, ZB, Tang, HL, Li DK, Tang, GJ. Vibration of single-layered graphene sheet-based nanomechanical sensor via nonlocal Kirchhoff plate theory. Comput Mater Sci 2012; 61: 200–205.

[12] Zenkour, AM. Nonlocal transient thermal analysis of a single-layered graphene sheet embedded in viscoelastic medium. Physica E 2016; 79: 87–97.

[13] Jiang, RW, Shen, ZB, Tang, GJ. Vibration analysis of single-layered graphene sheet-based mass sensor using Galerkin strip distributed transfer function method. Acta Mech 2016; 227: 2899–2910.

[14] Dastjerdi, Sh, Jabbarzadeh, M, Aliabadi, Sh. Nonlinear static analysis of single layer annular/circular graphene sheets embedded in Winkler Pasternak elastic matrix based on non-local theory of Eringen. Ain Shams Eng J 2016; 7: 873–884.

[15] Dastjerdi, Sh, Jabbarzadeh, M. Nonlinear bending analysis of bilayer orthotropic graphene sheets resting on Winkler-Pasternak elastic foundation based on non-local continuum mechanics. Compos Part B-Eng 2016; 87: 161–175.

[16] Dastjerdi, Sh, Jabbarzadeh, M. A Non-linear Static Equivalent Model for Multi-layer Annular/Circular Graphene Sheet Based on Non-local Elasticity Theory Considering Third Order Shear Deformation Theory in Thermal Environment. I J Eng Transactions B 2015; 28: 1533–1542.

[17] Liu, L. Defects in Graphene: Generation, Healing, and Their Effects on the Properties of Graphene. J Mech Sci Technol 2015; 31: 599–606.

[18] Dastjerdi, Sh, Aliabadi, Sh, and Jabbarzadeh, M. Decoupling of constitutive equations for multi-layered nano-plates embedded in elastic matrix based on non-local elasticity theory using first and higher order shear deformation theories. J Mech Sci Technol 2016; 30: 1253–1264.

[19] Dastjerdi, Sh, Lotfi, M, and Jabbarzadeh, M. The effect of vacant defect on bending analysis of graphene sheets based on the Mindlin nonlocal elasticity theory. Compos Part B-Eng 2016; 98: 78–87.

[20] Malikan, M, Jabbarzadeh, M, Dastjerdi, Sh. Non-linear static stability of bi-layer carbon nanosheets resting on an elastic matrix under various types of in-plane shearing loads in thermo-elasticity using nonlocal continuum. Microsyst Technol 2017; 23: 2973–2991.

[21] Ma, Y, Du, A, Hu, Y. The hysteresis loop and switching field in the bilayer film. P I Mech Eng-N: J of Nanoengineering and Nanosystems 2009; 222: 13–16.

[22] Naderi, A, and Saidi, AR. Common nonlocal elastic constitutive relation and material-behavior modeling of nanostructures. P I Mech Eng-N: J of Nanoengineering and Nanosystems 2017; 231: 83–87.

[23] Mohammadimehr, M, Mohammadi Najafabadi, MM, Nasiri, H, Rousta Navi, B. Surface stress effects on the free vibration and bending analysis of the nonlocal single-layer

graphene sheet embedded in an elastic medium using energy method. P I Mech Eng-N: J of Nanoengineering and Nanosystems 2014; 230: 148–160.

[24] Karimi, M, Shahidi, AR. Thermo-mechanical vibration, buckling, and bending of orthotropic graphene sheets based on nonlocal two-variable refined plate theory using finite difference method considering surface energy effects. P I Mech Eng-N: J of Nanoengineering and Nanosystems 2017; 231: 111–130.

[25] Ansari, R, Shahabodini, A, Alipour, A, and Rouhi, H. Stability of a single-layer graphene sheet with various edge conditions: a non-local plate model including interatomic potentials. P I Mech Eng-N: J of Nanoengineering and Nanosystems 2012; 226: 51–60.

[26] Lu, L, Ru, CQ, Guo, XM. Vibration of a multilayer graphene sheet under layerwise tension forces. Int J Mech Sci 2017; 121: 157–163.

[27] Nazemnezhad, R, Zare, M, Hosseini-Hashemi, S. Sandwich plate model of multilayer graphene sheets for considering interlayer shear effect in vibration analysis via molecular dynamics simulations. Appl Math Model 2017; 47: 459–472.

[28] Wu C-P, Li, W-C. Free vibration analysis of embedded single-layered nanoplates and graphene sheets by using the multiple time scale method. Comput Math Appl 2017; 73: 838–854.

[29] Allahyari E, Asgari, M. Thermo-mechanical vibration of double-layer graphene nanosheets in elastic medium considering surface effects; developing a nonlocal third order shear deformation theory. Eur J Mech A-Solid 2019; 75: 307-321.

[30] Hashemi, SH, Mehrabani, H, Ahmadi-Savadkoohi, A. Exact solution for free vibration of coupled double viscoelastic graphene sheets by viscoPasternak medium. Compos Part B-Eng 2015; 78: 377–383.

[31] Ansari, R, Motevalli, B, Montazeri, A, Ajori, S. Fracture analysis of monolayer graphene sheets with double vacancy defects via MD simulation. Solid State Commun 2011; 151: 1141–1146.

[32] Wang, Y-Z, Li, F-M, Kishimoto, K. Thermal effects on vibration properties of double-layered nanoplates at small scales. Compos Part B-Eng 2011; 42: 1311–1317.

[33] Allahyari, E, Asgari, M. Effect of magnetic-thermal field on nonlinear wave propagation of circular nanoplates. J Electromagnet Wave 2019; 42: 2296–2316.

[34] Giannopoulos, GI, Avntoulla, GS. Tensile strength of graphene versus temperature and crack size: Analytical expressions from molecular dynamics simulation data. P I Mech Eng-N: J Nanomaterials, Nanoengineering and Nanosystem 2017; 231: 67-73.

[35] Giannopoulos, GI. Crack Identification in Graphene Using Eigenfrequencies. Int J Appl Mech 2017; 9: 1750009.

[36] Hashimoto, A, Suenaga, K, Gloter, A, Urita K, Iijima S. Direct evidence for atomic defects in graphene layers. Nature 2004; 430: 870-873.

[37] Xiao, JR, Staniszewski, J, Gillespie Jr., JW. Fracture and progressive failure of defective graphene sheets and carbon nanotubes. Compos Struct 2009; 88: 602-609.

[38] Neek-Amal M, Peeters, FM. Linear reduction of stiffness and vibration frequencies in defected circular monolayer graphene. Phys Rev B 2010; 81: 235437.

[39] Tian, W, Li, W, Yu, W, Li, X, A Review on Lattice Defects in Graphene: Types, Generation, Effects and Regulation. Micromachines 2017; 8: 163.

[40] Lee, JH, Avsar, H, Jung, J, Tan, JY, Watanabe, K, Taniguchi, T, Natarajan, S, Eda, G, Adam, Sh, Castro Neto, AH, Özyilmaz, B. van der Waals Force: A Dominant Factor for Reactivity of Graphene. Nano Lett 2015; 15: 319− 325.

[41] Jomehzadeh, E, Saidiac, AR, Pugno, NM. Large amplitude vibration of a bilayer graphene embedded in a nonlinear polymer matrix. Physica E 2012; 44: 1973-1982.

[42] Farajpour, A, Arab Solghar, A, Shahidi, A. Postbuckling analysis of multi-layered graphene sheets under non-uniform biaxial compression. Physica E 2013; 44: 197-206.

[43] Wang, J, He, X, Kitipornchai, S, Zhang, H. Geometrical nonlinear free vibration of multi-layered graphene sheets. J Phys D Appl Phys 2011; 44: 135401.

[44] Lu, WB, Wu, J, Song, J, Hwang, KC, Jiang, LY, Huang, Y. A cohesive law for interfaces between multi-wall carbon nanotubes and polymers due to the van der Waals interactions. Comput Method Appl M 2008; 197: 3261-3267.

[45] Zhang, YP, Challamel , N, Wang, CM, Zhang, H. Comparison of nano-plate bending behaviour by Eringen nonlocal plate, Hencky bar-net and continualised nonlocal plate models. Acta Mech 2019; 230: 885–907.

[46] Alibeigloo, A, Shaban, M. Free vibration analysis of carbon nanotubes by using three-dimensional theory of elasticity. Acta Mech 2013; 224: 1415–1427.

[47] Alipour, MM, Shaban, M. Bending analysis of multi-layered graphene sheets under combined non-uniform shear and normal tractions. J Solid Mech 2017; 9: 12–23, 2017.

[48] Lazar, M, Agiasofitou, E, Po, G. Three-dimensional nonlocal anisotropic elasticity: a generalized continuum theory of Ångström-mechanics. Springer Vienna, 2019.

[49] Dastjerdi, Sh, Akgöz, A, Civalek, Ö. On the effect of viscoelasticity on behavior of gyroscopes. Int J Eng Sci 2020; 149: 103236.

Figure Captions

Fig. 1. Schematic view of Winkler-Pasternak medium and van der Waals interaction (a) and geometrical view of the defect (b)

Fig. 2. Maximum deflection of upper and bottom layers versus k_o

Fig. 3. R_m for upper and bottom layers versus k_o

Fig. 4. Maximum deflection of upper and bottom layers versus eccentricity for (a) different values of k_w (b) k_p

Fig. 5. Maximum deflection of upper and bottom layers versus eccentricity for different values of nonlocal parameter

Fig. 6. Variation of R_m for upper and bottom layers versus eccentricity for different values of nonlocal parameter

Fig. 7. Variation of R_v for upper and bottom layers versus nonlocal parameter

Fig. 8. Variation of maximum deflection for upper and bottom layers versus r_i for different values of nonlocal parameter

Fig. 9. Linear and nonlinear deflection results of bilayer defected graphene sheet

List of Tables

Fig. 1

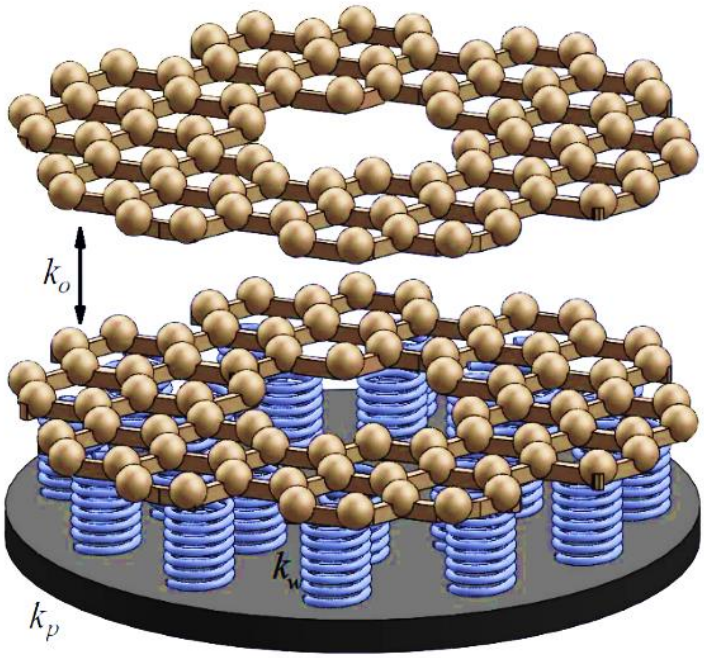

(a)

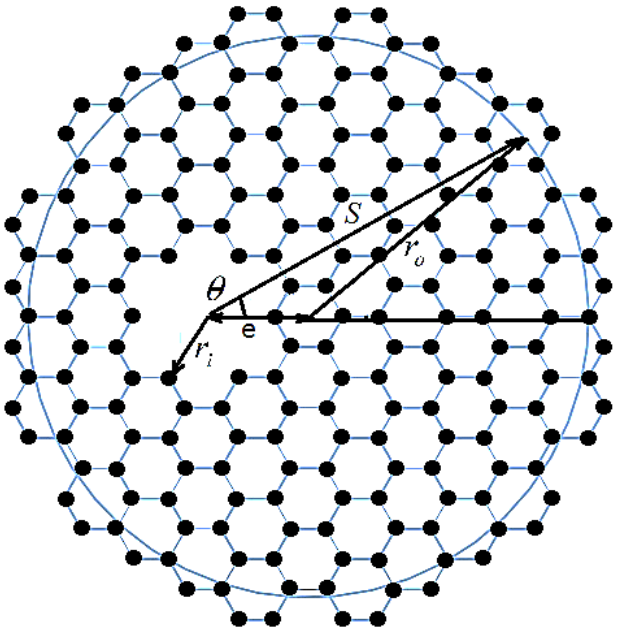

(b)

Fig. 2

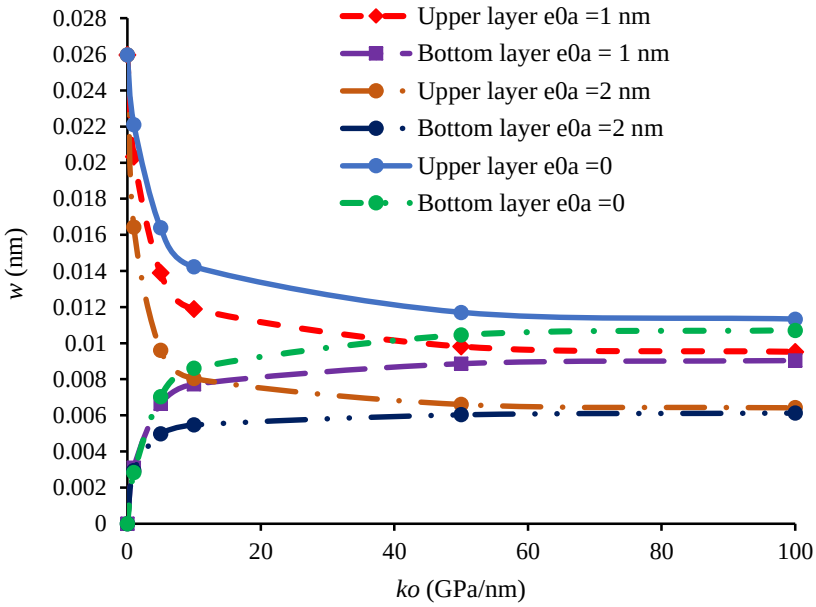

Fig. 3

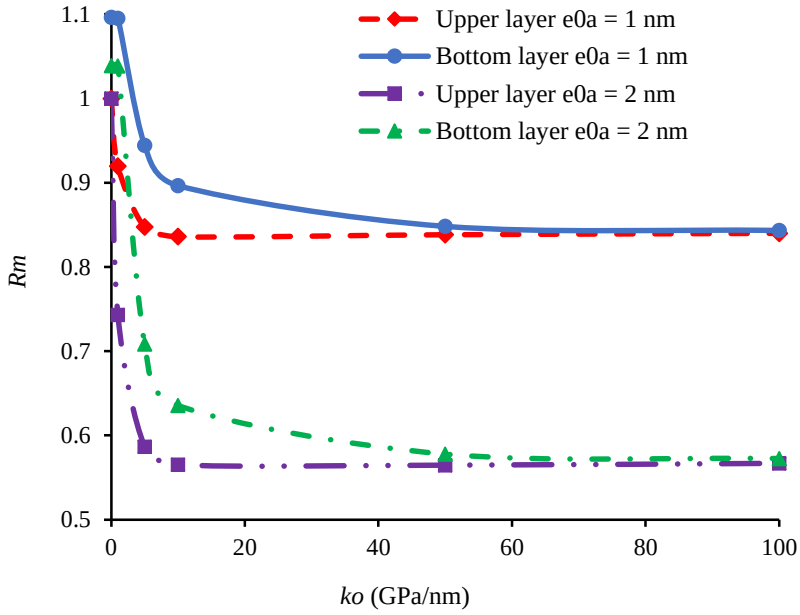

Fig. 4

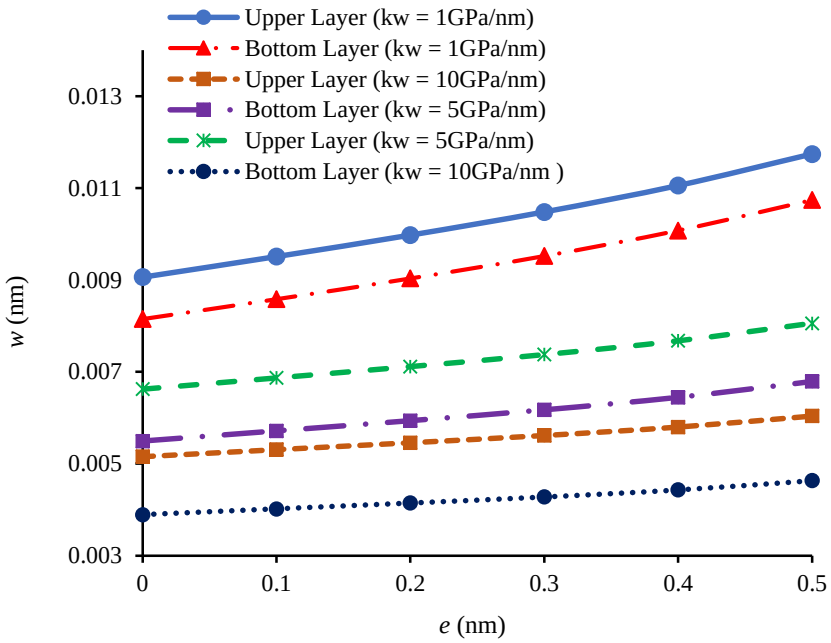

(a)

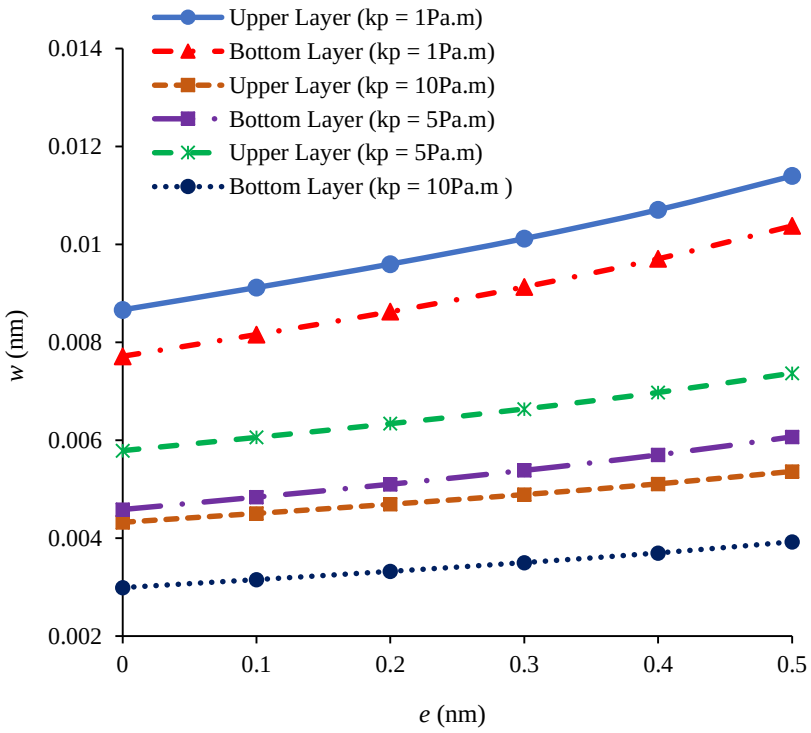

(b)

Fig. 5

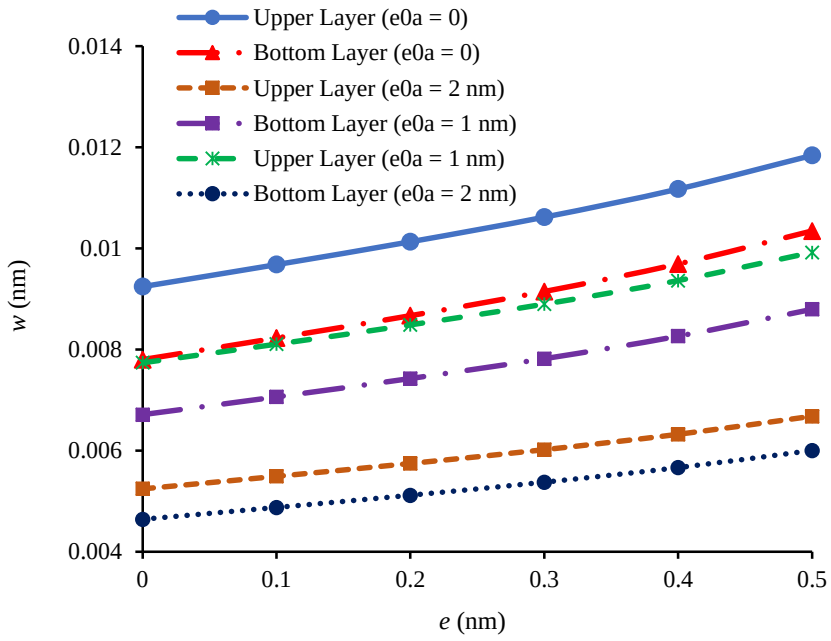

Fig. 6

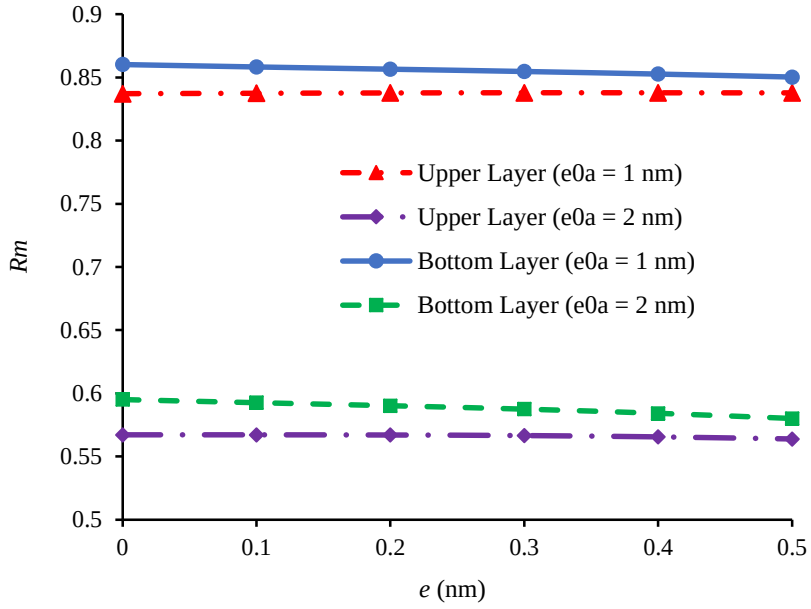

Fig. 7

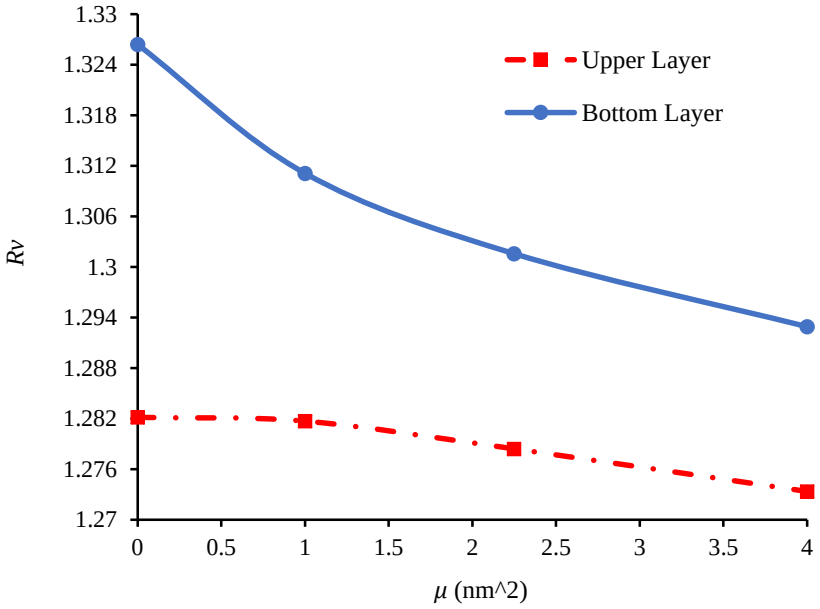

Fig. 8

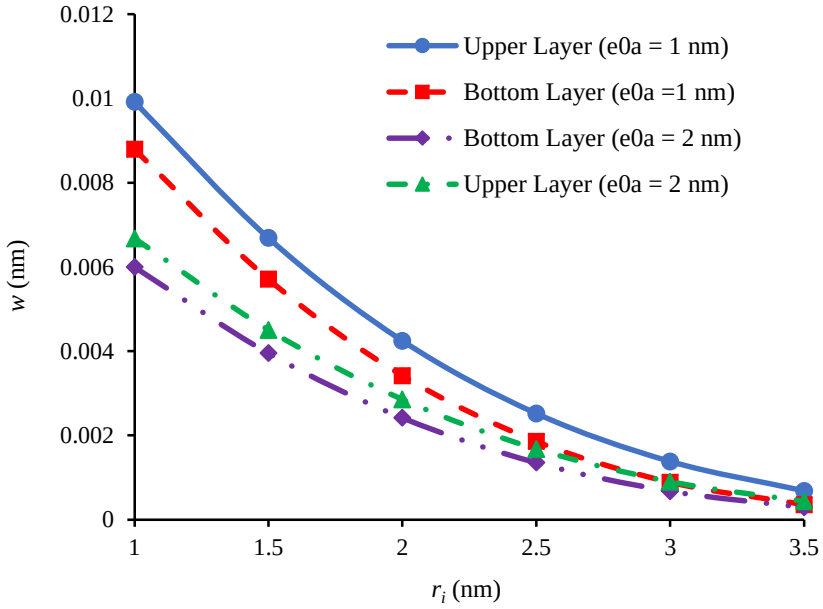

Fig. 9

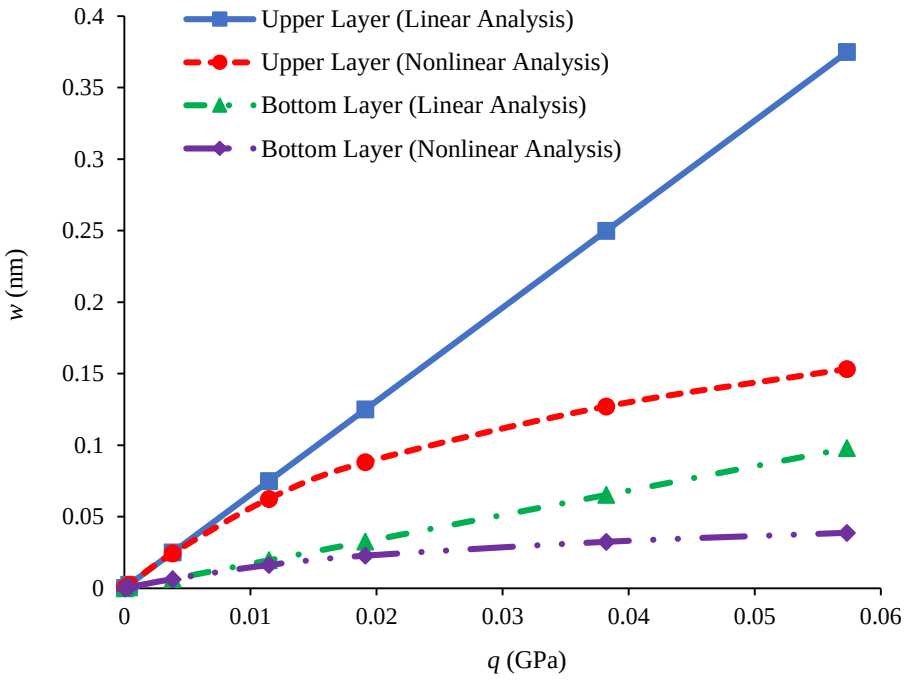

Table 1. Maximum deflection obtaining in the present paper and ABAQUS for a circular macro plate

BCs	e (m)	w (mm)				
		ABAQUS				Present
		Elements=6500	13000	30000	50000	
CC	0	0.03862	0.03902	0.03933	0.03933	0.03936
	0.05	0.05972	0.06032	0.06090	0.06090	0.05757
	0.1	0.08747	0.08839	0.08910	0.08910	0.08611
	0.15	0.12250	0.12370	0.12435	0.12435	0.1121
	0.2	0.16460	0.16596	0.16678	0.16678	0.1507
FC	0	0.57170	0.57392	0.57592	0.57592	0.5711
	0.05	0.60771	0.61020	0.61261	0.61261	0.5895
	0.1	0.61642	0.61952	0.62213	0.62213	0.6012
	0.15	0.59870	0.60258	0.60484	0.60484	0.5773
	0.2	0.56261	0.56509	0.56712	0.56712	0.5467

Table 2. Comparison between the results of present paper and Ref [14]

	w / r_o	
$e_0 a\,(\mathrm{nm})$	[14]	Present
0	0.003063	0.003069
0.5	0.002985	0.002990
1	0.002774	0.002778
1.5	0.002484	0.002487
2	0.002170	0.002173